Hindawi
Geofluids
Volume 2021, Article ID 5569525, 21 pages
https://doi.org/10.1155/2021/5569525

WILEY | Hindawi

Research Article

Investigation on Acoustic Emission Kaiser Effect and Frequency Spectrum Characteristics of Rock Joints Subjected to Multilevel Cyclic Shear Loads

Zhiqiang Hou,[1,2] **Changhong Li**,[1,2] **Zhengyang Song**,[1,2] **Yonggang Xiao**,[1,2] **Chen Qiao**,[1,2] **and Yu Wang**[1,2]

[1]*Key Laboratory of Ministry of Education for High-Efficient Mining and Safety of Metal Mines, University of Science and Technology Beijing, Beijing 100083, China*
[2]*School of Civil and Resource Engineering, University of Science and Technology Beijing, Beijing 100083, China*

Correspondence should be addressed to Yu Wang; wyzhou@ustb.edu.cn

Received 26 January 2021; Revised 21 February 2021; Accepted 28 February 2021; Published 14 March 2021

Academic Editor: Zhigang Tao

Rock joints have obvious acoustic emission (AE) Kaiser effect and Felicity effect under multilevel cyclic shear conditions. The TFD-20H/50J rock shear apparatus was used to carry out cyclic loading and unloading joint shear tests, and the acoustic emission parameters and frequency spectrum characteristics of the whole shearing process were analyzed. The results show that, under the cyclic loading, the shear stress-displacement curve forms several cyclic hysteresis loops, and the number of loops increases with the increase of normal stress. With the cycles increase, the shear damage gradually increases, and the Felicity ratio gradually decreases. The Felicity ratio at the final shear failure moment is about 0.94~0.99. The ratio of the RA value (rise time/amplitude) and the average frequency value (RA-AF) is used to classify the cracking mode of the joint sample. There are two AE crack signal types (tensile type and shear type) during shear damage. The peak frequency is displayed as high, medium, and low three frequency bands, which are distributed in the range of 0~35 kHz, 35~122 kHz, and 122~300 kHz, respectively. Both low-frequency and high-frequency signals account for less than 10%, and medium-frequency signals account for more than 90%. The research of the AE monitoring signals of multilevel shear behaviors can help understand the shear-friction mechanisms of rock joints.

1. Introduction

The deformation failure mechanism and slope instability mechanism of mine rock slopes in alpine area have always been the focus of mine disaster prevention research. Due to the influence of the harsh natural environment, the rock mass of the slope usually produces discontinuous, irregular, and heterogeneous rock joints. After being affected by rock mass excavation, mine blasting, vehicle loads [1], or earthquakes, the structural surfaces of rock masses often close and slip under the action of cyclic load, which seriously affects the structural integrity and stability of the rock slopes [2, 3]. Therefore, it is necessary to conduct a deep study on the jointed rock mass under cyclic shear load.

In the laboratory research of cyclic loading and unloading experiments, Kaiser first discovered the acoustic emission stress memory function of polycrystalline metal in 1950 [4, 5] and Goodman [6] proved that the rock also has the Kaiser effect during loading. The Kaiser effect of acoustic emission means that during the unloading process, no obvious acoustic emission event generating, and once the stress reaches the previously largest reached stress, the AE activity would increase dramatically [7–10], that is, the rock has the ability to remember the stress information experienced in the past. The Kaiser effect often appears at a stress level not exactly equal, but a little higher or lower than the previous largest stress of load. Such advanced or delayed memory properties are usually estimated by Felicity ratio (FR value) [11–13],

which is the ratio of the stress with generating obvious acoustic emission activity to the previous peak stress, as shown in equation (1).

$$\mathrm{FR} = \frac{\sigma_{\mathrm{AE}}}{\sigma_{i-1}}. \quad (1)$$

In the formula, FR is the Felicity ratio, i is the i-th cycle; σ_{AE} is the stress of Kaiser effect point, and σ_{i-1} is the previous maximum stress.

Felicity ratio is an indicator of the material damage severity. Generally speaking, the FR value is between 0.9 and 1.1. As the FR value decreases, the material damage degree becomes larger. In some composite materials, the FR value less than 0.95 is usually used as an important criterion for the material damage [14].

Afterwards, many scholars expounded the influencing factors of Kaiser effect from different perspectives, including stress level, time delay, loading rate, confining pressure, rock heterogeneity, and loading direction in cyclic loading and unloading test. Lavrov [8, 9] pointed out that the memory stress of rock Kaiser effect is closely related to the time delay between loading cycles. The longer the time delay, the more fully crack development, the more significant the Kaiser effect during reloading. Lavrov also pointed out that in brittle rocks, the Kaiser effect begins to occur when the rock is subjected to a stress level of 70%-80% (when dilatancy begins) [10]. However, in ductile rocks, Kaiser effect can be observed in the whole loading range [15]. Furthermore, the water saturation, heating, or loading rate [16, 17] of rock can also reduce the discriminability of the Kaiser effect. Larger loading rate can shorten the crack propagation time, inhibit the propagation of small cracks in the rock, reduce the acoustic emission events, and finally lead to an increase in the FR value. When the loading rate is low, the stress producing significant AE activity is usually lower than the previous maximum historical stress, while at a high loading rate, the stress is close to the maximum historical stress, which is the reason that the large loading rate is recommended to estimate the in situ stress in engineering [12]. In addition, the Kaiser effect is highly sensitive to rotation in the loading direction [18]. When the repeated loading direction is different from the initial loading direction, the Kaiser effect of the rock will gradually weaken or even degenerate and disappear.

The identification and differentiation of acoustic emission frequency spectrum are the key content in the field of material microfracture research. The acoustic emission source signal analysis is now mainly based on the AE correlation parameter method and the waveform spectrum analysis method. Based on the parameter classification method, the characteristic relationship between the acoustic emission RA value (rise time/amplitude) and the average frequency can better reflect the types of crack, which is regarded as a criterion to classify the tensile crack and shear crack [19–23]. Based on the spectrum feature analysis method, the time domain signal of the waveform is usually converted into frequency domain signal by means of fast Fourier transform (FFT) [24–26]. According to the peak frequency distribution characteristics of acoustic emission signals, the purpose of AE source crack pattern recognition can be achieved.

At present, the research on acoustic emission waveform and frequency spectrum characteristics of rock mainly focuses on compression aspect [27–32], and the frequency spectrum analysis had also been carried out on the direct tensile test [33], the Brazilian tensile test [34], and three-point bending test [35, 36]. However, there are few reports on the Kaiser effect and spectrum analysis of rock joint shear test. Therefore, it is necessary to have a deep study about the multistage cyclic shear test of rock joints to further systematically and comprehensively understand the acoustic emission mechanism of shear failure.

2. Specimens and Methods

2.1. Specimen Preparation of Rock Joints. The rock studied was skarn, obtained from the western slope of the Beizhan open-pit iron mine in Xinjiang, Northwestern China, as shown in Figure 1. The local climate is the continental temperate semiarid climate, high mountains are covered with snow all year round, and the altitude of the mining area is 3450-3730 m. The temperature in winter is cold, with a minimum temperature of -40°C; in summer, the temperature has a big difference between day and night, with a maximum temperature of about 20°C during the day and a temperature of -5°C at night. After continuous freezing, thawing, and weathering, the rocks are mostly fragmented. The microfractures in the rock are developed, the physical and mechanical properties are reduced, and discontinuities are generally formed (joints, cracks, bedding planes, faults, block structures, and other fractures). The natural density of rock is 2.73 g/cm^3, wave velocity is 5682 m/s, uniaxial compressive strength is 81.3 MPa, and Poisson's ratio is 0.29.

The samples were cut from a single block of skarn. Considering the size of the shear box, the sample is shaped and trimmed into a cuboid of 100 mm length, 60 mm width, and 60 mm height. The joint samples were split from the middle of the cuboid in the laboratory, thus forming two samples of equal size [37]. The untested samples were fixed into the mold and cured with encapsulating material at 20°C and 90% relative humidity for more than 28 days. The joint surface height is approximately 5 mm higher than the encapsulating material surface height. After the sample was prepared, the direct shear test can be carried out under constant normal load (CNL) condition according to the ISRM recommended methods [38].

2.2. Experimental Scheme and Test Apparatus

2.2.1. Rock Joint Shear Testing System. The direct shear test was carried out with the TFD-20H/50J rock joint shearing apparatus under constant normal load (CNL) conditions at the University of Science and Technology Beijing, as shown in Figure 2. The shearing machine has a rated normal force of 20 kN, a rated shear force of 50 kN, a normal stroke of 100 mm, and a tangential stroke of 200 mm. It is equipped with a rigid test box that is symmetrical up and down and is equipped with a sensitive load and deformation testing

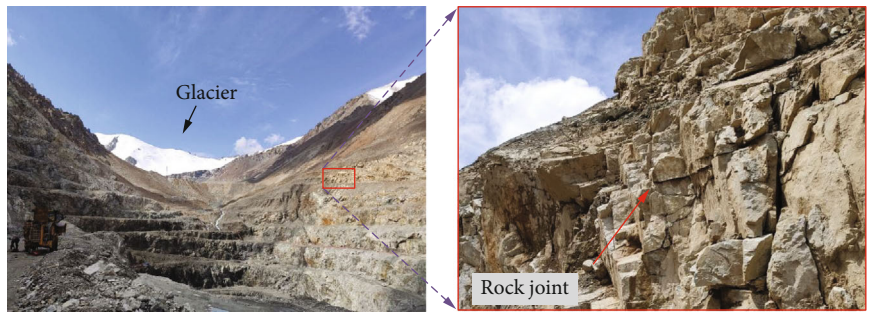

Figure 1: Rock joint sample collection: (a) high elevation slope and (b) massive block structure with rich joints of the natural slope.

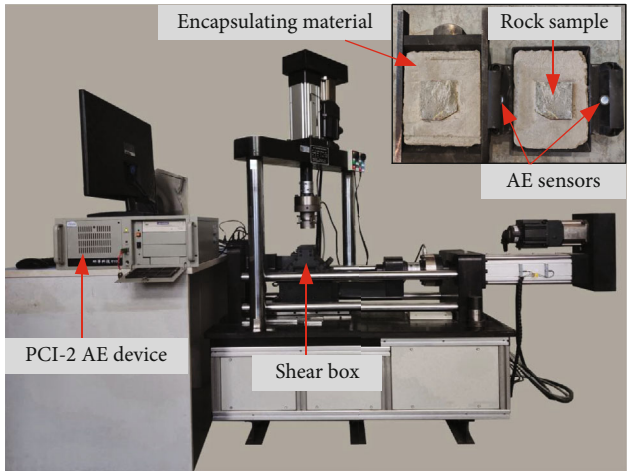

Figure 2: Rock shear testing system and PCI-2 acoustic emission device.

device. According to the method recommended by ISRM [38], the upper and lower parts of rock joint were, respectively, perfused in shear boxes with encapsulating material. The rock joint sliding in nature condition is often repeated. With the influence of geological tectonic stress or production activities, the normal stress on the joint surface is likely to increase or decrease. The shear test for a piece of rock is more consistent with the slope sliding phenomenon.

Figure 3 shows an overview of the test scheme, including applied normal stress, applied shear stress, and designed loading path. In this multilevel shear test, one same rock sample was tested under four normal stresses. The normal forces were 5 kN, 7.5 kN, 10 kN, and 12.5 kN, respectively, which the corresponding normal stresses were 1.39 MPa, 2.08 MPa, 2.78 MPa, and 3.47 MPa. The loading rate of the normal displacement was 0.02 mm/s. When the normal load reaches the predetermined load, the shear load can be applied. During the shearing process, the upper shear box was remained fixed, and the lower shear box was moved under the control of lateral loading axis. First, load the shear strength to a set value at a shear rate of 2 mm/min and then unload it to 1 kN at the same rate to complete a cycle. Then, increase the shear strength step by step until the residual shear strength of joint was reached. After each shearing, the joint samples were adjusted and reset to make the upper and lower surfaces match each other; then, we can carry out a next test. The whole shearing process was automatically controlled by the software, and the test data could be automatically recorded and saved. After the test, the normal axis was raised and the test sample can be taken out.

2.2.2. AE Testing Approach. Acoustic emission technique was used to monitor the friction damage of rock joints during the whole shearing process. Based on the AE test theory, a series of AE signal parametric features, including AE ringing counts, rise time, amplitude, duration time, average frequency, peak frequency or accumulated trend, are customarily used for characterizing the damage degree of materials. The PCI-2 acoustic emission monitor can completely record AE waveforms and AE characteristic parameters in the damage process of material, which is a high-performance acoustic emission system developed by the American Physical Acoustics Corporation (PAC), as shown in Figure 2. The system has a built-in 18-bit A/D converter and processor, with a frequency bandwidth of 1 kHz-3 MHz, which is suitable for low-amplitude, low-threshold signal monitoring. The sampling frequency in this shearing test was set at 1 MHz, the threshold level was set at 35 dB, and the amplification gain was set at 40 dB. The acoustic emission sensor was an RS-2A sensor with a resonance frequency of 150 kHz. Specific steps of acoustic emission monitoring are as follows:

(1) *Arrange the Sensors*. Two acoustic emission sensors were arranged outside of the lower shear box. The area of the sensor arrangement needs to be properly cleaned, and an appropriate amount of Vaseline was applied to the sensor surface, and the sensor should be gently squeezed to make the sensor and the shear box completely contact.

(2) *Set the AE Monitoring Parameters*. Open the acoustic emission software, adjust the receiving channel, and set the monitoring frequency range and threshold value.

(3) *Pretrigger Debugging*. Perform short-time signal acquisition on the instrument to ensure that the connectivity between the probe, data line, and the acoustic emission instrument is intact well before starting the acoustic emission test.

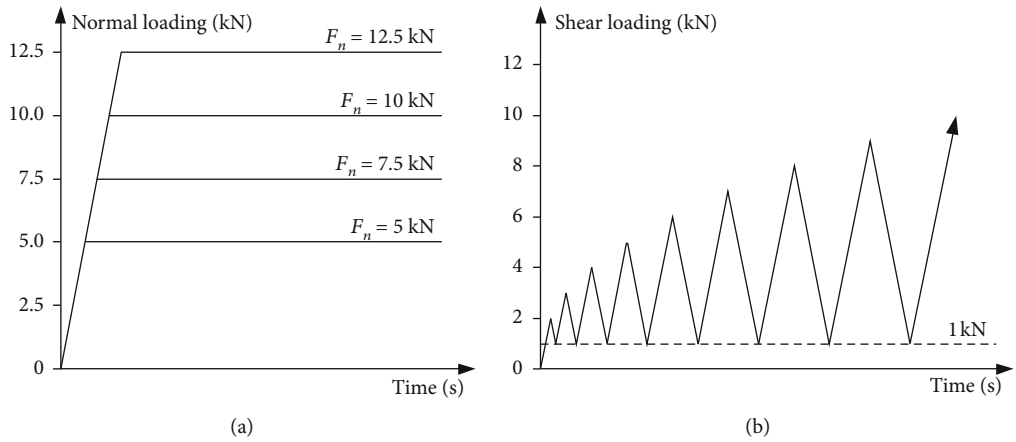

Figure 3: The designed loading path under CNL condition. (a) The set normal force of 5 kN, 7.5 kN, 10 kN, 12.5 kN. (b) Multilevel cyclic shear loading path.

2.3. Theory of Acoustic Emission Crack Classification. Acoustic emission is a phenomenon caused by stress concentration in a material local area, rapidly releasing energy and generating transient elastic waves [39, 40]. AE events are generated by fracture phenomena and are identified by the electrical signals which are amplified, filtered, and processed. The frequency domain, amplitude, and frequency characteristics of signals vary greatly with the material type, and different materials need to consider different working frequencies. For example, the frequency domain of metal materials is about several kilohertz to several megahertz, composite materials are about several kilohertz to hundreds of kilohertz, and rock and concrete are about several hertz to hundreds of kilohertz [41].

AE signal source types are classified by the use of AE parameters, such as count, amplitude, rise time, duration, frequency, or the related parameter distribution characteristics. In rock and concrete materials, the classification of crack types is proposed, using the ratio between the RA value (rise time/amplitude) and the average frequency (AF) value. This classification method has been used and standardized in nondestructive testing [42–44]. The expressions for RA value and AF value are clearly shown in the following equations.

$$\begin{aligned} \text{RA value} &= \frac{\text{Rise time}}{\text{Amplitude}}, \\ \text{AF value} &= \frac{\text{Counts}}{\text{Duration}}. \end{aligned} \tag{2}$$

The combination of four AE parameters reflects two cracking behaviors: the tensile type and the shear type. It is well known that in rock or concrete structures, tensile motion occurs when cracks nucleate or opening, and frictional motion occurs when fretting or sliding over existing cracks. Generally speaking, AE activities of tensile cracks are usually observed in the stable stage of fracture growth, as approaching the final failure, AE activities of shear cracks are observed. The AE signal classification between tensile crack and shear-friction crack is shown in Figure 4. In general, the mode of tensile cracks mostly has low RA value and high AF value, while the mode of shear cracks have the characteristics of high RA value and low AF value. However, there is still no definite signal ratio for how to accurately distinguish the tensile crack from the shear crack. It is more often distinguished by the inherent characteristics of materials or by empirical relationships [45]. In the field of brittle materials such as concrete, the ratio of the RA value and the AF value for crack classification is usually set at 1 : 8000~10 : 1 according to different test methods [23]. Once the relationship ratio is determined, no matter how large or small the value is, it can well show the change trend of the tensile and shear signals.

3. Results and Analysis

3.1. Shear Strength Curves. Figure 5 shows the normal force-time curve of four shear tests. Curves show that the normal force remains unchanged with only sporadic jitter, which conforms to the CNL test standard.

Figure 6(a) shows the shear stress versus shear displacement curves of the rock joint cyclic shear behaviors, and Figure 6(b) shows the partial enlargement of the curve under the condition of $\sigma_n = 3.47$ MPa. The shear strength of each curve is in the range of 71%~84% to the corresponding normal stress. The shear strength parameters are summarized in Table 1. Four stress-displacement curves all form several cyclic hysteresis loops. As the normal stress increases, the number of hysteresis loops increases. Among them, four hysteresis loops are formed under the condition of $\sigma_n = 1.39$ MPa, five hysteresis loops are formed under the condition of $\sigma_n = 2.08$ MPa, five hysteresis loops are formed under the condition of $\sigma_n = 2.78$ MPa, and seven hysteresis loops are formed under the condition of $\sigma_n = 3.47$ MPa. The descending curve and the ascending curve of each hysteresis loop are close to overlap, and the slopes of the two curves are approximately equal, which means that the resistances to the joint movement in the positive and negative directions are the same. Besides, if ignore the cyclic hysteresis loop of the shear curve, when the shear stress increases again, the shear curve will continue to rise monotonously along the original "expected" trajectory and will not be affected by

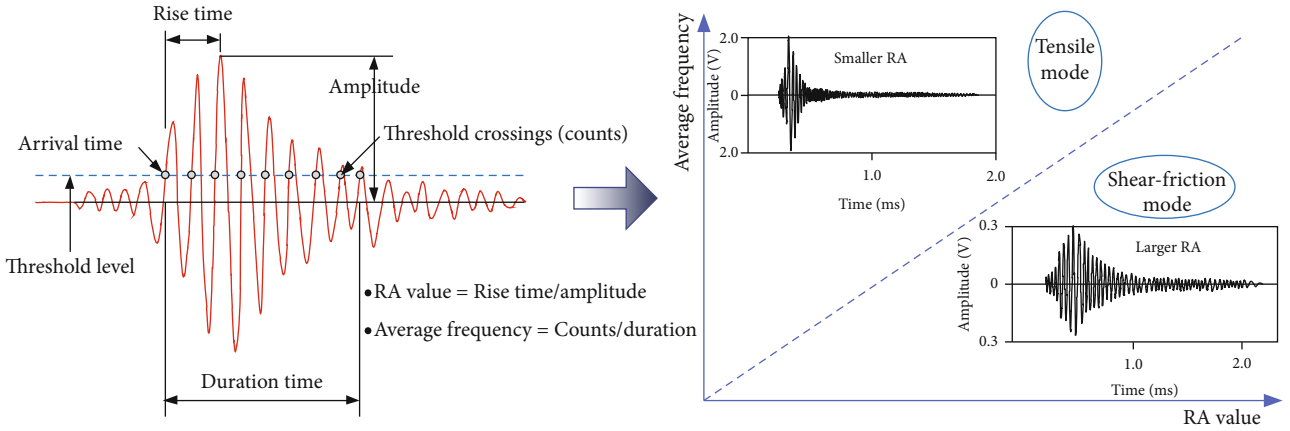

Figure 4: AE signal classification of tensile crack and shear-friction crack.

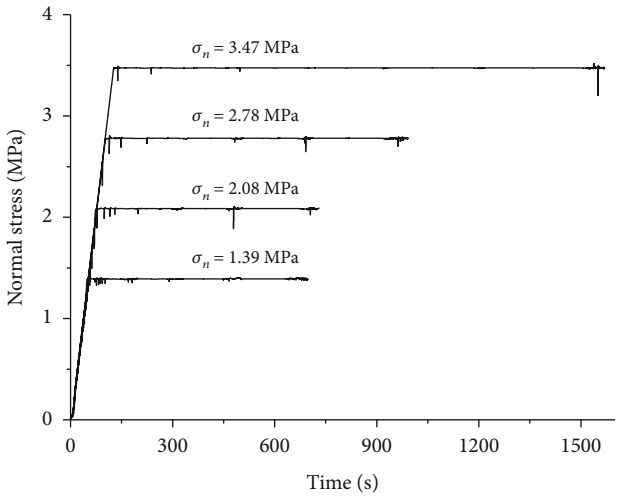

Figure 5: Normal stress-time curves.

the loading path, that is, the joint rock has a memory ability of shear deformation.

3.2. Felicity Ratio of Cycle Loading. Figure 7 shows the relationship between the shear stress, AE count rate, AE accumulative counts, and the test time for skarn joint under four normal stresses. The shear stress-time curve reflects the macroscopic mechanical characteristics of skarn specimens, while the acoustic emission count-time curve provides the severity of rock shear damage [46]. During the download and upload processes of each cycle curve (without exceeding the previous maximum shear force), acoustic emission events are rarely generated. Once the previous maximum stress is exceeded, continuous acoustic emission events occur. Accordingly, the shear cycle loading and unloading processes have an obvious Kaiser effect. From the AE count rate curves and AE cumulative count curves, it can be seen that the AE activity under low normal stress (σ_n = 1.39 MPa) is significantly greater than that under high normal stresses. That is because the sample used was the same rock. The rock joint would produce intense acoustic emission events during the first cycle shearing, but for repeated more cycle shearing, the joint surface would become smoother, and fewer acoustic emission events would occur.

At present, how to judge a "significant" emission for determining the Kaiser effect point has no uniform standard, usually based on a matter of experience. American Society of Testing Materials (ASTM) had given three recommendations [14]: (1) more than five bursts of emission during a 10% increase in load; (2) more than half of total duration value during a 10% increase in load, where the duration value is determined by a pencil lead broken test; (3) emission continues at a load hold.

The Felicity ratio of the cyclic shear process under different normal stresses is calculated by equation (1). Figure 8 and Table 2 show the FR variations under different normal stresses. The FR value generally decreases with cycle number increasing. In the first two cycles, the FR value is greater than or close to 1, and in the subsequent cycles, the FR value is less than 1. For σ_n = 1.39 MPa, the Felicity effect appears when the relative stress of the third cycle is 87.18%, and the FR value is 0.99; for σ_n = 2.08 MPa, the Felicity effect appears when the relative stress of the third cycle is 74.83%, and the FR value is 0.99; for σ_n = 2.78 MPa, the Felicity effect appears when the relative stress of the fourth cycle is 69.19%, and the FR value is 0.98; for σ_n = 3.47 MPa, the Felicity effect appears when the relative stress of the second cycle is 43.65%, and the FR value is 0.98. That is, the greater the normal stress, the easier it is to achieve the stress conditions of Felicity effect.

In summary, the Felicity effect is generated in the latter part of the shearing process, and the RF value before rock failure is about 0.94~0.99. In engineering applications, analyzing the size of the Felicity ratio can measure the force state of the rock. If the RF value is close to 1, it indicates that the rock damage is getting more serious, and the rock is close to the failure strength. Sufficient attention should be paid to avoid the occurrence of engineering geological disasters.

Figure 9 shows the morphology damage features of jointed skarn. Owing to the effect of shear friction, uneven symmetrical scratches are left on the joint surface after shearing. The high convex parts of the joint surface were cut off,

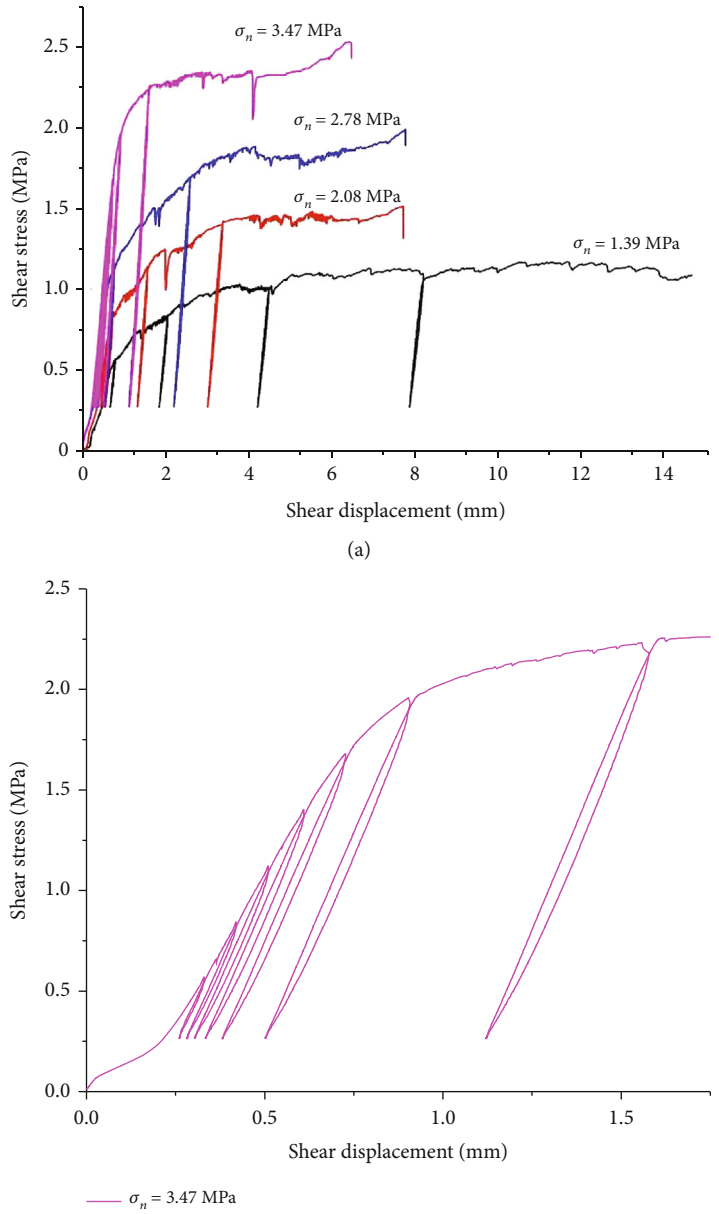

Figure 6: Shear stress versus shear displacement curves. (a) Cyclic shear behaviors of rock joints with constant normal stress of 1.39 MPa, 2.08 MPa, 2.78 MPa, and 3.47 MPa; (b) partial enlarged view of curve with a constant normal stress of 3.47 MPa.

Table 1: Shear strength parameters under different normal force conditions.

Rock joint type	Normal force F_n (kN)	Normal stress σ_n (MPa)	Shear loading rate (mm/min)	Number of cyclic hysteresis loop	Shear strength τ (MPa)	τ/σ_n (%)
Joint of skarn (length × width × height, 60 × 60 × 50 mm)	5.0	1.39	2.0	4	1.17	83.84%
	7.5	2.08	2.0	5	1.51	72.77%
	10.0	2.78	2.0	5	1.98	71.38%
	12.5	3.47	2.0	7	2.52	72.70%

and the low concave areas were filled with powdery rock debris. A few large rock particles were produced at the joint surface edge, and the particle diameters ranged from 1 mm to 15 mm. After shear test, the joint surface is more close to flat and much smoother, and the roughness of surface is significantly reduced.

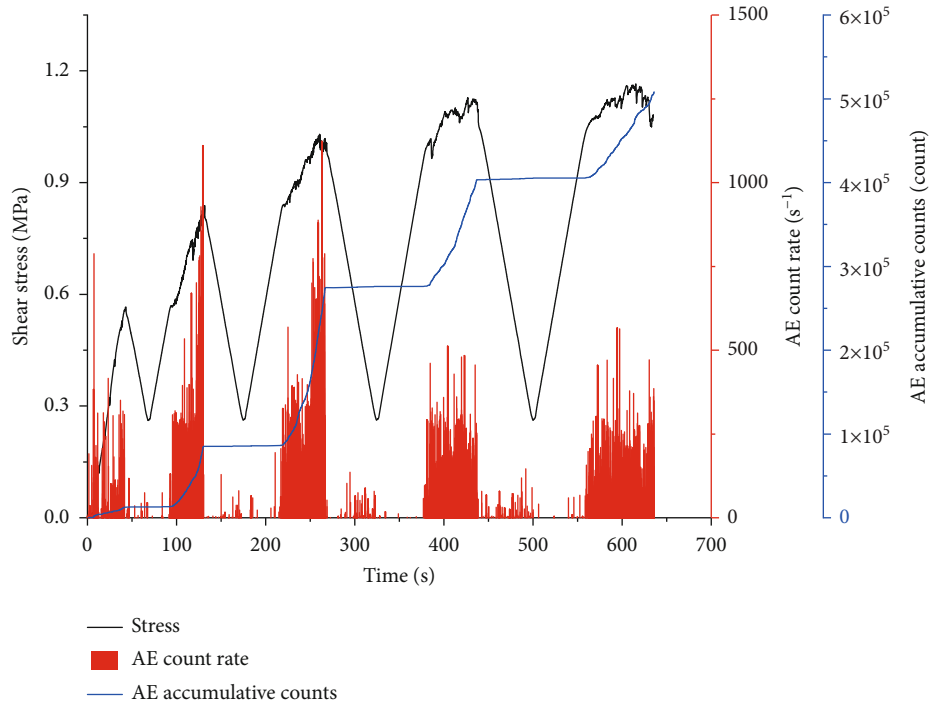

(a) σ_n = 1.39 MPa

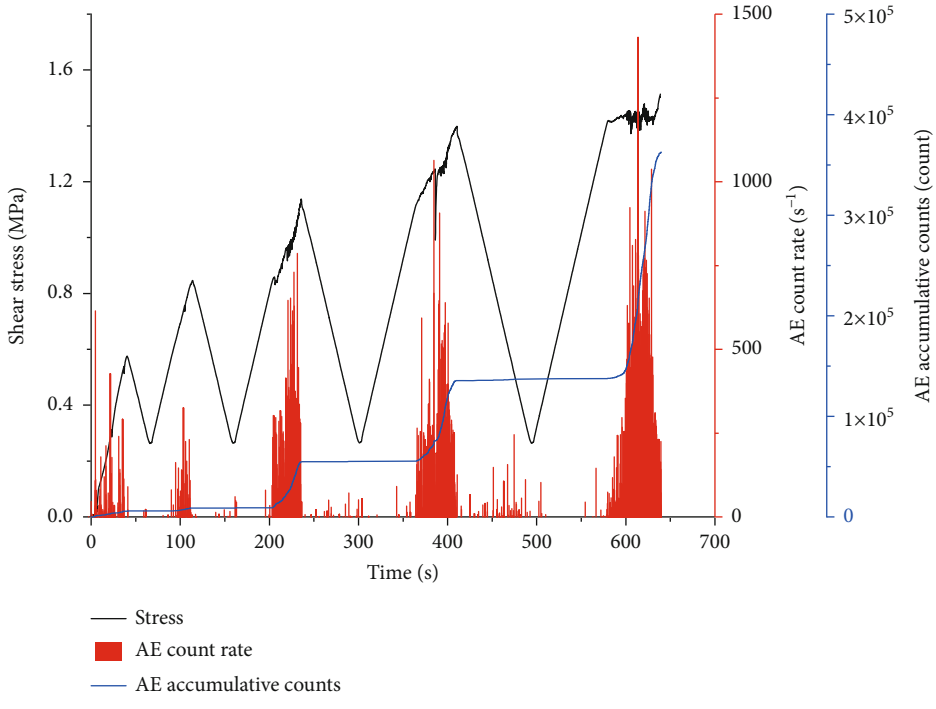

(b) σ_n = 2.08 MPa

Figure 7: Continued.

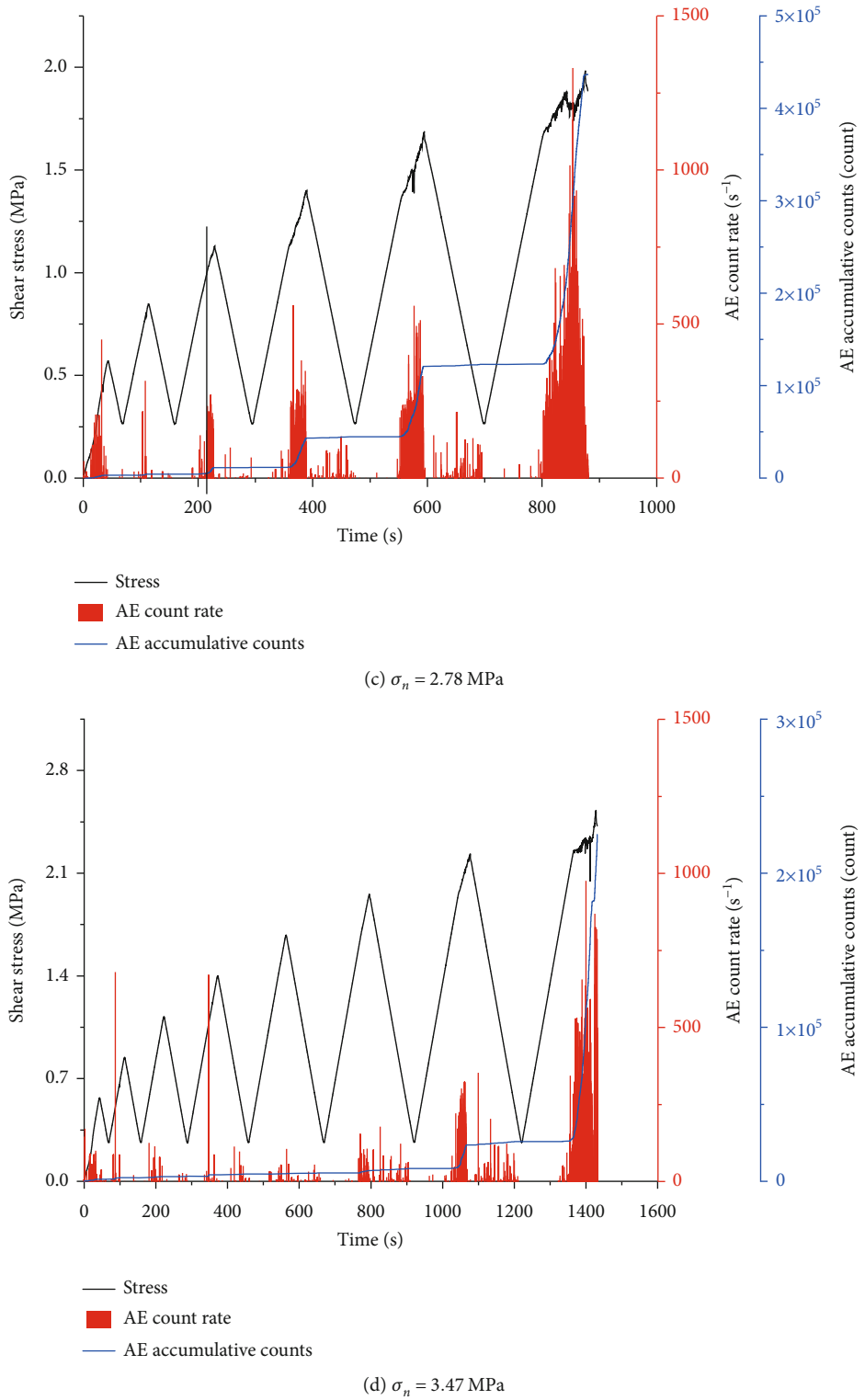

Figure 7: The relationship between the shear stress, AE count rate, AE accumulative counts, and the test time for skarn joints under normal stress of 1.39, 2.08, 2.78, and 3.47 MPa, respectively.

3.3. AE Classifications of Tensile Crack and Shear Crack Signals. Figure 10 shows the AE crack classification 3D results of the shearing progress of rock samples at different normal stresses. Figure 11 shows the signal distribution projection results on the average frequency axis and the RA value axis. The RA value is distributed in the range of 0~120 ms/V, and the average frequency is distributed in the range of 0~500 kHz. In this article, we set the ratio of the RA and the AF value of crack classification to 1 : 10 and use this signal ratio to distinguish the tensile signal from the shear signal.

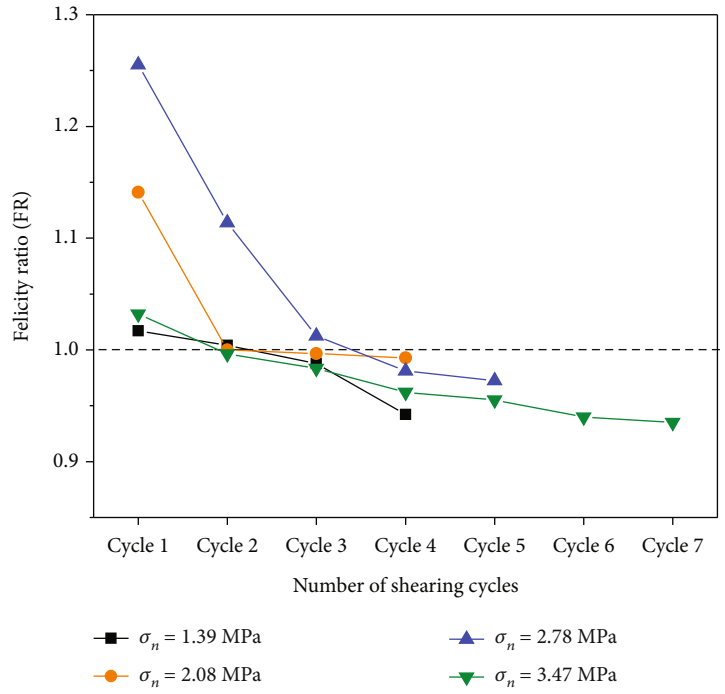

Figure 8: Felicity ratio variations under four normal stress of 1.39 MPa, 2.08 MPa, 2.78 MPa, and 3.47 MPa, respectively.

Table 2: Felicity ratios under different normal stress.

Cycle No.	σ_n = 1.39 MPa	σ_n = 2.08 MPa	σ_n = 2.78 MPa	σ_n = 3.47 MPa
	Peak stress in each cycle/MPa, Kaiser stress/MPa, and Felicity ratio (FR)			
1	0.57, 0.58, 1.02	0.58, 0.66, 1.14	0.57, 0.72, 1.26	0.57, 0.59, 1.03
2	0.84, 0.84, 1.00	0.85, 0.85, 1.00	0.85, 0.95, 1.11	0.84, 0.84, 1.00
3	1.03, 1.02, 0.99	1.14, 1.13, 0.99	1.13, 1.14, 1.01	1.12, 1.10, 0.98
4	1.13, 1.06, 0.94	1.40, 1.39, 0.99	1.40, 1.37, 0.98	1.40, 1.35, 0.96
5			1.69, 1.64, 0.97	1.68, 1.60, 0.96
6				1.95, 1.83, 0.94
7				2.23, 2.09, 0.94

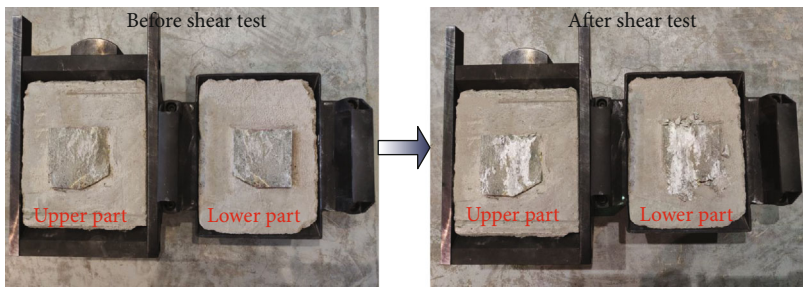

(a) (b)

Figure 9: Upper and lower parts of jointed skarn specimens: (a) before shear test and (b) after shear test.

Figure 10 intuitively shows that the number of AE signals under low normal stress is obviously higher than that under high normal stress. This phenomenon has been mentioned in Section 3.2, and the reason is that the joint surface becomes smoother with the increase of the cycle number, so that causes the number of acoustic emission signals to decrease after multiple shears.

To further analyze the number of acoustic emission tensile signals and shear signals, as well as the AE signal trend changes, we conducted a statistical quantification for each

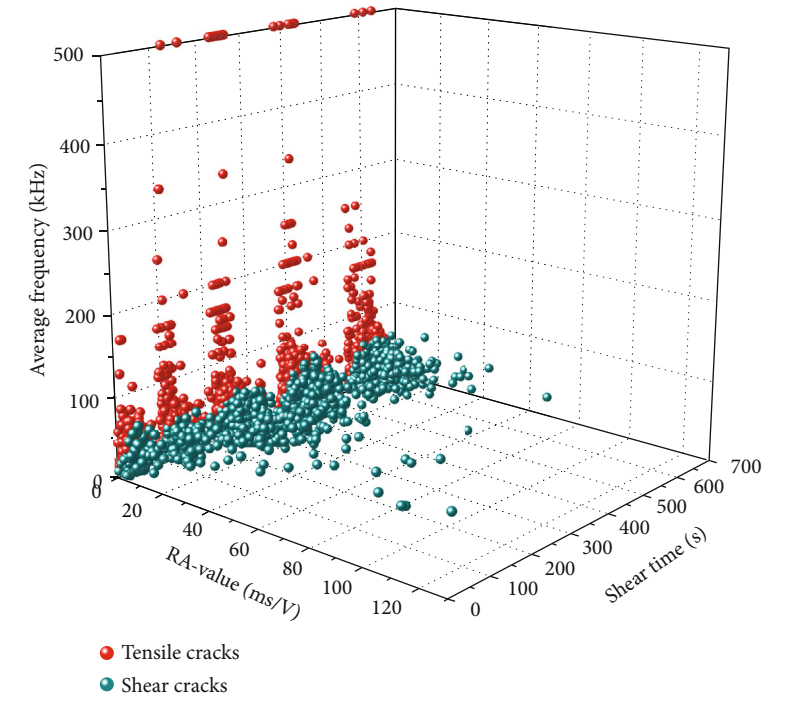

(a) $\sigma_n = 1.39$ MPa

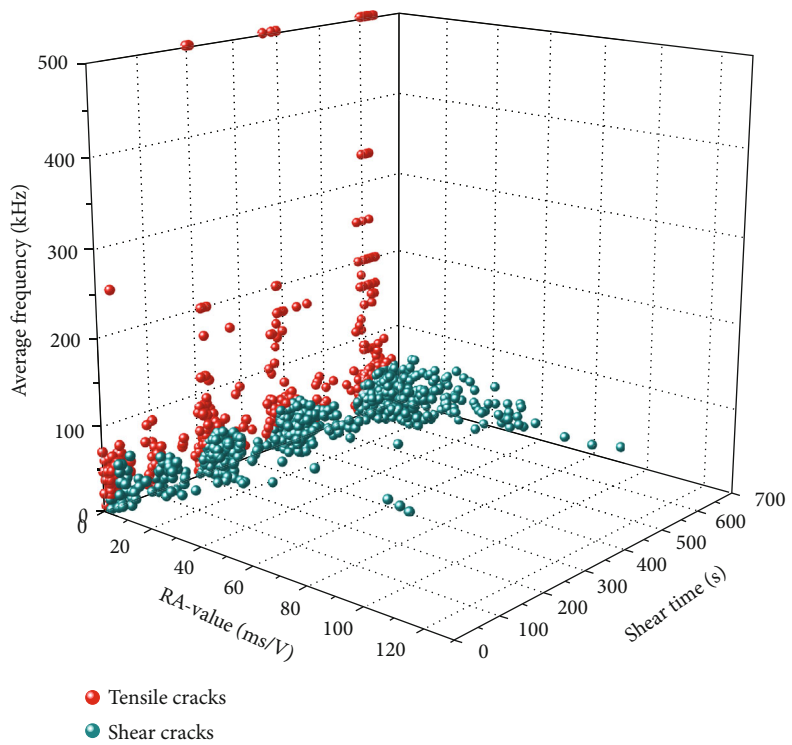

(b) $\sigma_n = 2.08$ MPa

Figure 10: Continued.

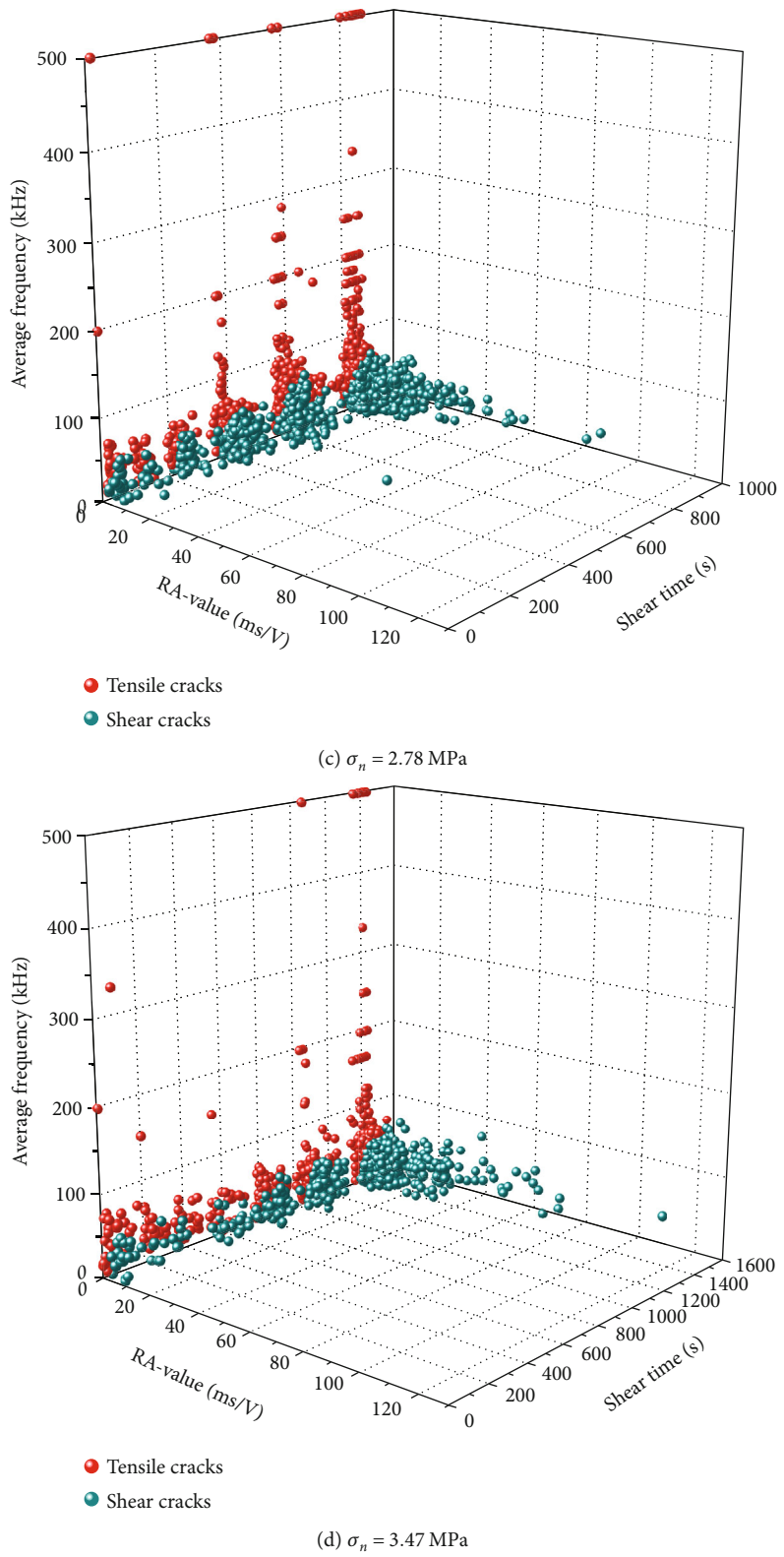

Figure 10: Signal evolution of the tensile cracks and shear cracks at different normal stress levels.

cycle based on the ratio value of RA : AF (RA : AF = 1 : 10), and the statistical results of the signals are shown in Table 3, and the signal variation trends are shown in Figure 12.

In the cyclic shearing process under four normal stresses, the acoustic emission signal of skarn joints has three signal characteristics. (1) For different normal stress shear tests, the tensile signal is dominant during the first cycle shearing,

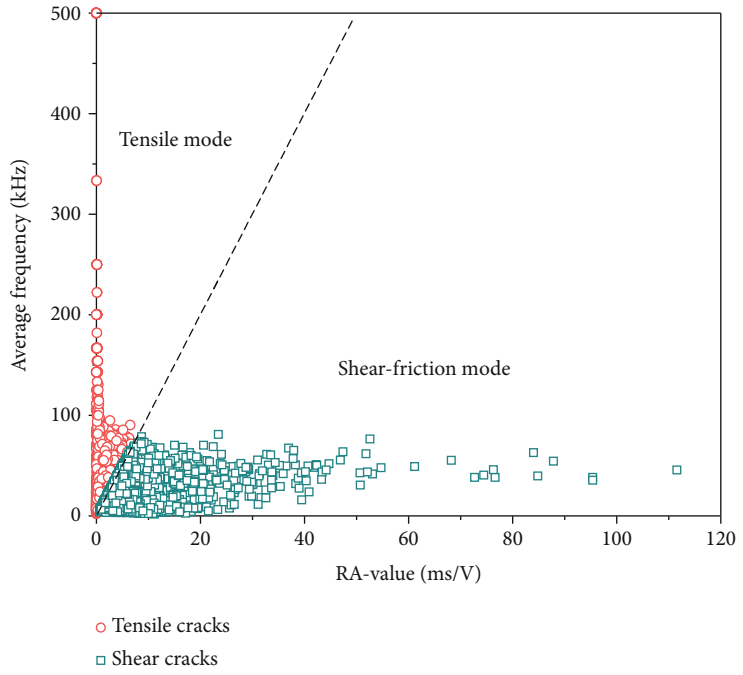

(a) $\sigma_n = 1.39$ MPa

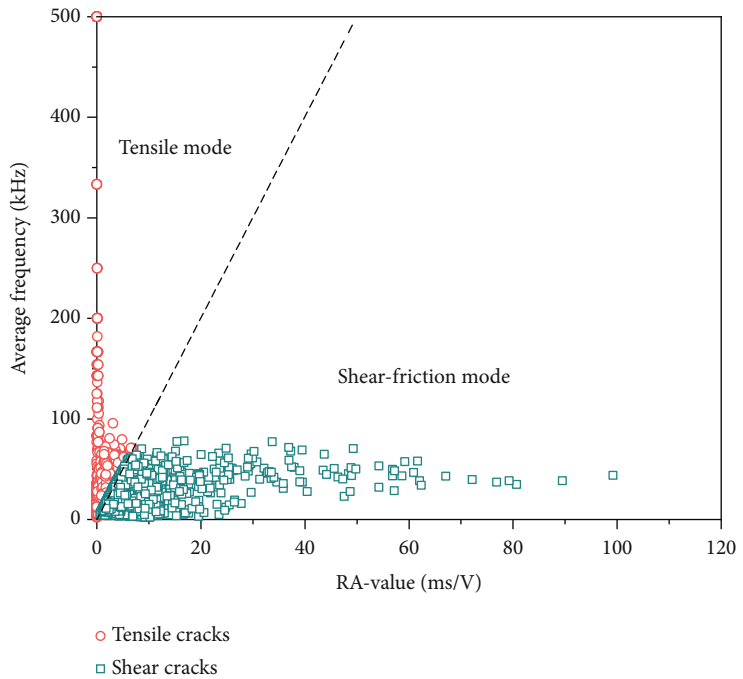

(b) $\sigma_n = 2.08$ MPa

Figure 11: Continued.

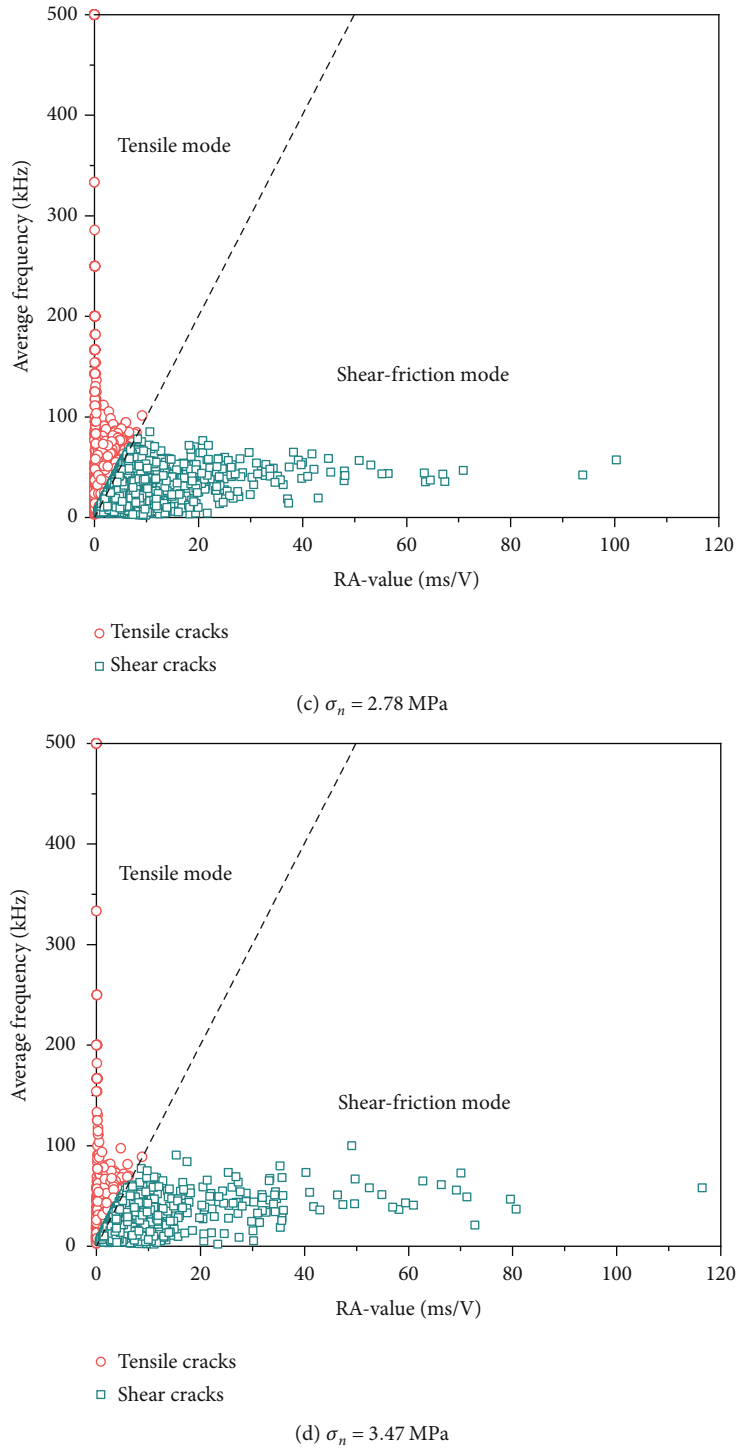

Figure 11: Signal distributions of tensile and shear cracks under different normal stress levels, which the ratio of the RA and the AF value is set to 1 : 10.

while the shear signal is dominant during the last cycle shearing. (2) With shear cycles increase, the proportion of tensile signals gradually decreases and the proportion of shear signals gradually increases. Especially when the normal stress is equal to 1.39 MPa, this trend is particularly obvious in the cyclic shearing process due to the joint surface sheared for the first time. (3) In a complete cyclic shear process, the number of tensile signals generated is less than that of shear signals. When $\sigma_n = 1.39$ MPa, the proportions of tensile signal and shear signal are 40.8% and 59.2%, respectively. When $\sigma_n = 2.08$ MPa, the proportions of tensile signal and shear signal are 45.9% and 54.1%, respectively. When $\sigma_n = 2.78$ MPa, the proportions of tensile signal and shear signal are 44.2% and 55.8%, respectively. When $\sigma_n = 3.47$ MPa, the proportions of tensile signal and shear signal are 46.1% and 53.9%, respectively.

Table 3: Statistical distribution results of tensile and shear signals in each cycle.

Number of cycle	(a) σ_n = 1.39 MPa			(b) σ_n = 2.08 MPa			(c) σ_n = 2.78 MPa			(d) σ_n = 3.47 MPa		
	Tensile signal	Shear signal	Total signal	Tensile signal	Shear signal	Total signal	Tensile signal	Shear signal	Total signal	Tensile signal	Shear signal	Total signal
Cycle 1	114 (54.3%)	96 (45.7%)	210	68 (65.4%)	36 (34.6%)	104	30 (52.6%)	27 (47.4%)	57	30 (63.8%)	17 (36.2%)	47
Cycle 2	384 (46.9%)	434 (53.1%)	818	30 (47.6%)	33 (52.4%)	63	19 (59.4%)	13 (40.6%)	32	5 (41.7%)	7 (58.3%)	12
Cycle 3	1062 (40.3%)	1576 (59.7%)	2638	284 (46.2%)	331 (53.8%)	615	45 (41.7%)	63 (58.3%)	108	22 (73.3%)	8 (26.7%)	30
Cycle 4	974 (39.5%)	1492 (60.5%)	2466	533 (52.4%)	484 (47.6%)	1017	241 (43.7%)	311 (56.3%)	552	18 (72.0%)	7 (28.0%)	25
Cycle 5	725 (39.0%)	1134 (61.0%)	1859	1240 (42.8%)	1660 (57.2%)	2900	588 (47.8%)	641 (52.2%)	1229	22 (48.9%)	23 (51.1%)	45
Cycle 6							1811 (43.1%)	2392 (56.9%)	4203	49 (51.6%)	46 (48.4%)	95
Cycle 7										166 (47.7%)	182 (52.3%)	348
Cycle 8										1225 (44.8%)	1508 (55.2%)	2733
Total	3259 (40.8%)	4732 (59.2%)	7991	2155 (45.9%)	2544 (54.1%)	4699	2734 (44.2%)	3447 (55.8%)	6181	1537 (46.1%)	1798 (53.9%)	3335

3.4. Distribution of AE Peak Frequency. Based on the signal analysis of AE events (or cumulative parameters) in time domain and frequency domain, we can get the activity performances of rock acoustic emission events. In this paper, AE data were processed by using discrete Fourier transform, and the frequency spectrums of waveform signals were obtained. For a discrete AE event $f(t)$ at a given time t, it can be decomposed by its Fourier transform $F(w)$ [24, 26], that is,

$$f(t) = \frac{1}{2\pi}\int_{-\infty}^{+\infty} F(w)e^{iwt}dw,$$
$$F(w) = \int_{-\infty}^{+\infty} f(t)e^{-iwt}dt, \tag{3}$$

where $f(t)$ and $F(w)$ are a pair of Fourier transforms. $F(w)$ is independent of time and represents the frequency composition of a random process. Assuming that the AE signal $f(t)$ contains N points, the corresponding discrete Fourier sums [25] can be expressed as

$$\widehat{f}(k) = \sum_{n=0}^{N-1} f(n)e^{-(2\pi kn/N)(j)}(0 < k < N), \tag{4}$$

where $\widehat{f}(k)$ represents the FFT algorithm. Therefore, the frequency spectrum characteristics and dominant peak of $f(t)$ can be obtained by the FFT.

Frequency domain characteristics are often intrinsic and unique, ranging from microscopic particles to objects in the macroscopic world and even celestial bodies, all of which have inherent frequency characteristics. The uniqueness of the frequency spectrum can well reflect the fracture characteristics inside the rock, such as the crack initiation and propagation, and all deformation of material has corresponding frequencies and amplitudes. In the AE frequency distribution diagram, the area with dense frequency distribution can be defined as the main frequency band or the intrinsic frequency. In general, the AE frequency is inversely proportional to the crack size. Small-scale cracks accompanied with high-frequency signals, and large-scale cracks accompanied with low-frequency signals [27, 28]. Spectrum analysis is actually to obtain the essential characteristics of AE signals in the frequency domain for the information that cannot be found in the time domain.

Figure 13 and Table 4 show the AE peak frequency with amplitude distributions. For the shear tests under the four normal stresses, although the normal stresses are different, the distribution of peak frequency information is the same, and 99% of the frequencies are distributed in 5~170 kHz. The peak frequency is displayed as high, medium, and low three frequency bands, which ranges are 5~35 kHz, 35~122 kHz, and 122~ 170 kHz, respectively. The distributions of these three bands are concentrated and clearly visible, as shown in Figure 13. In the whole shearing process, the proportion of low- and high-frequency signals is relatively small, both proportions are less than 10%. The proportion of medium-frequency signals is large, reaching more than 90%. Meanwhile, with the normal stress increase, the proportion of high-frequency signals gradually decreases, and the proportion of medium-frequency signals gradually increases, while the proportion of low-frequency signals does not change significantly. The decrease of high-frequency signal indicates that the fracture of small cracks gradually disappear, while the increase of medium-frequency signal indicates that the shear-slip and friction of large cracks are

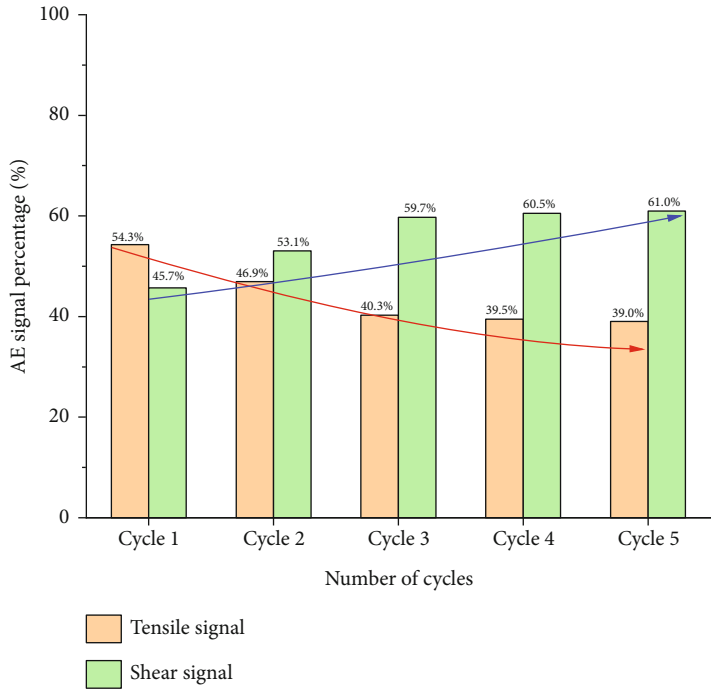

(a) $\sigma_n = 1.39$ MPa

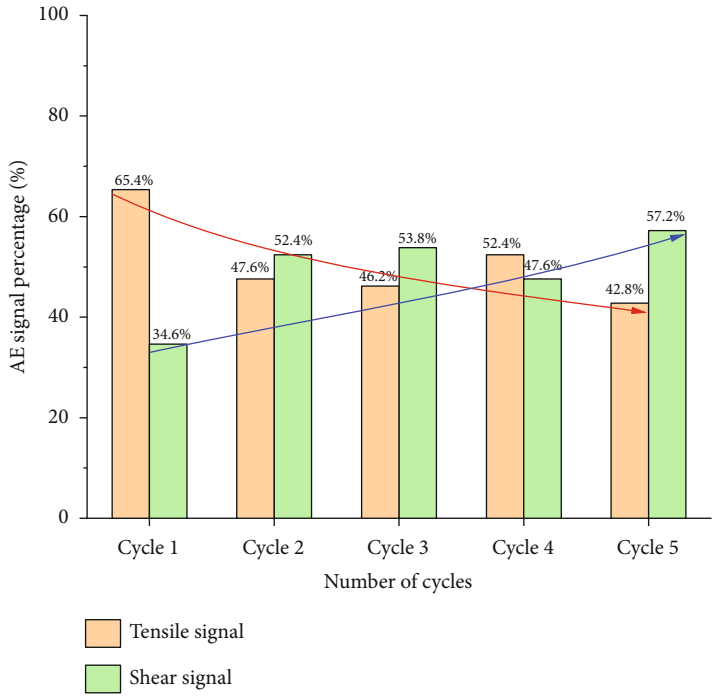

(b) $\sigma_n = 2.08$ MPa

Figure 12: Continued.

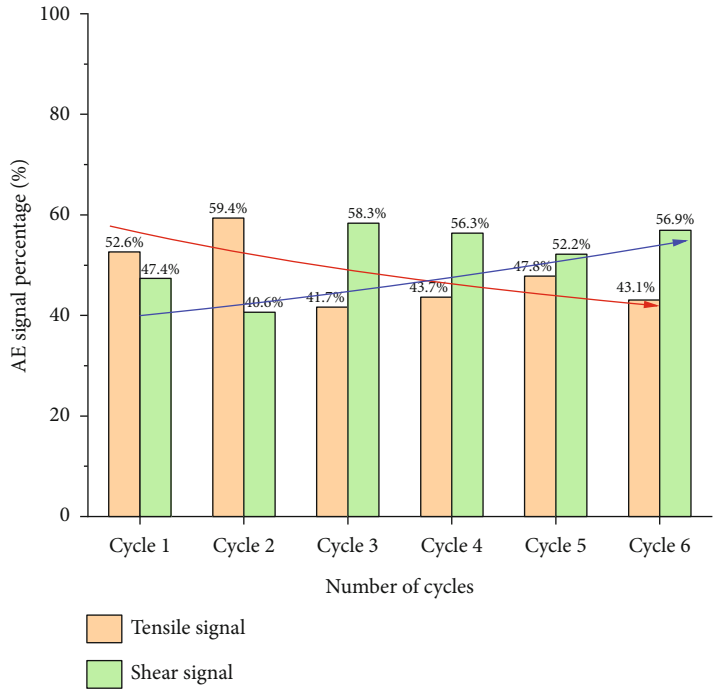

(c) $\sigma_n = 2.78$ MPa

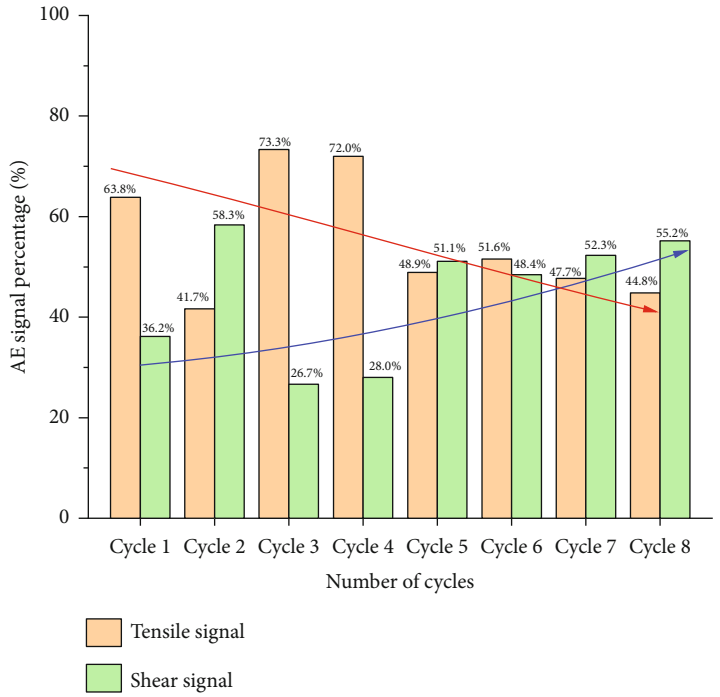

(d) $\sigma_n = 3.47$ MPa

FIGURE 12: The proportion variation trend of the tensile signal and the shear signal in the cyclic shear process under four normal stresses.

increasing, indicating that the damage is gradually aggravated. This also verifies the change rule in Section 3.3 that with the increase of normal stress, the tensile cracks decrease and the shear cracks increase.

3.5. Frequency Spectrum Characteristics of AE Signal. In each shear test, the acoustic emission monitor had received thousands of AE waveform signals. After classifying and counting these signals, it can be found that there are mainly one type of tensile signal and three types of friction signals during the whole shearing process, as shown in Figure 14. The tensile signal is mainly a burst-rupture type signal, as shown in Figure 14(a), which is characterized by high frequency and low amplitude, usually occur at the early stage of shear test, indicating a crack initiation behavior. The three friction signals have low-frequency characteristics and are divided

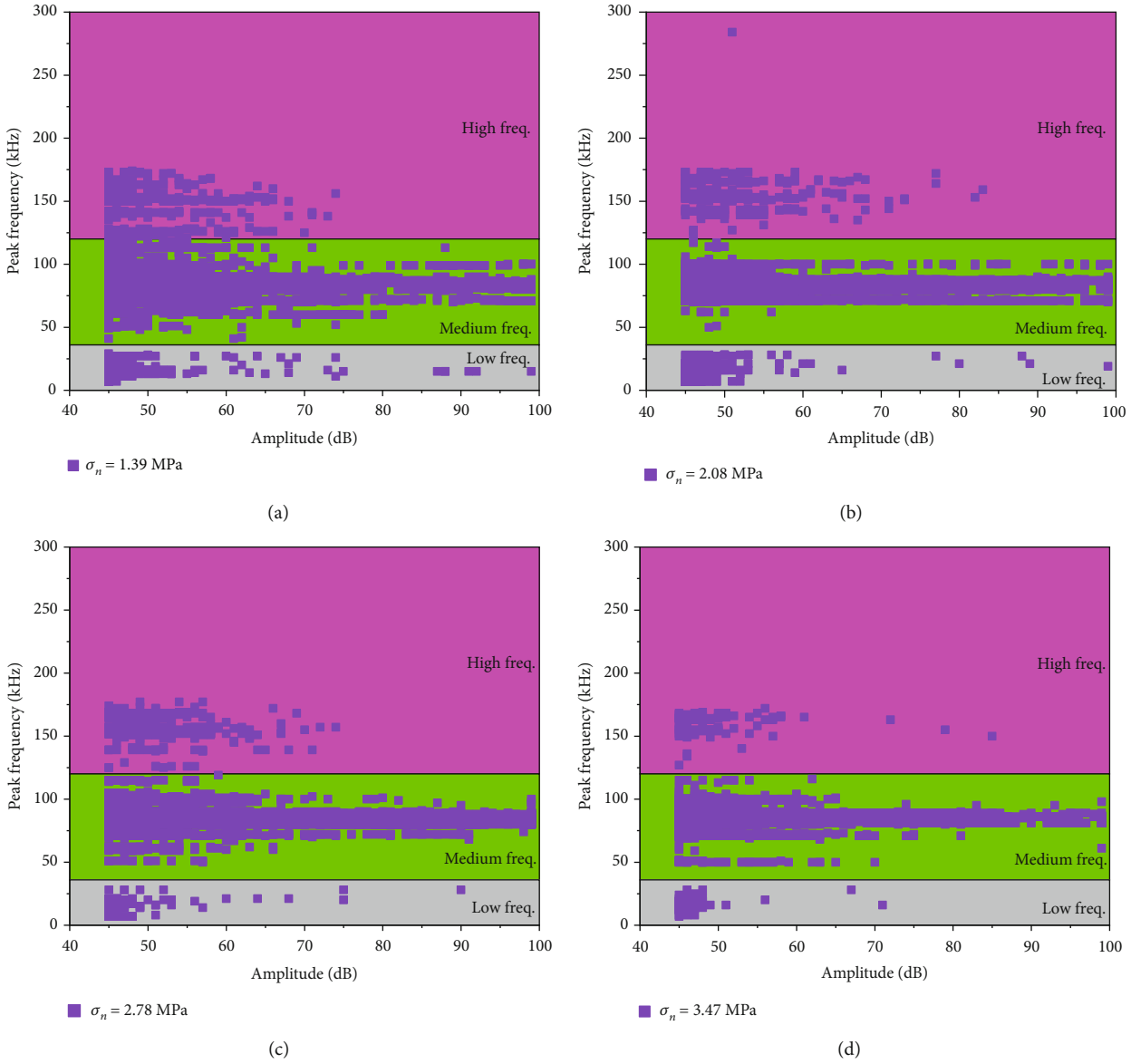

Figure 13: The frequency and amplitude distribution characteristics of rock joint shearing under four normal stresses.

Table 4: Percentage of AE signals of low, medium, and high frequencies in the rock shearing process under four normal stresses.

Normal stress σ_n/MPa	Low freq./number	Medium freq./number	High freq./number	Total signal/number	Low freq. signal/% (0~35 kHz)	Medium freq. signal/%(35~122 kHz)	High freq. signal/%(122~300 kHz)
σ_n = 1.39 MPa	272	8705	563	9540	2.85%	91.25%	5.90%
σ_n = 2.08 MPa	224	5734	305	6263	3.58%	91.55%	4.87%
σ_n = 2.78 MPa	149	6758	299	7206	2.07%	93.78%	4.15%
σ_n = 3.47 MPa	59	3783	80	3922	1.50%	96.46%	2.04%

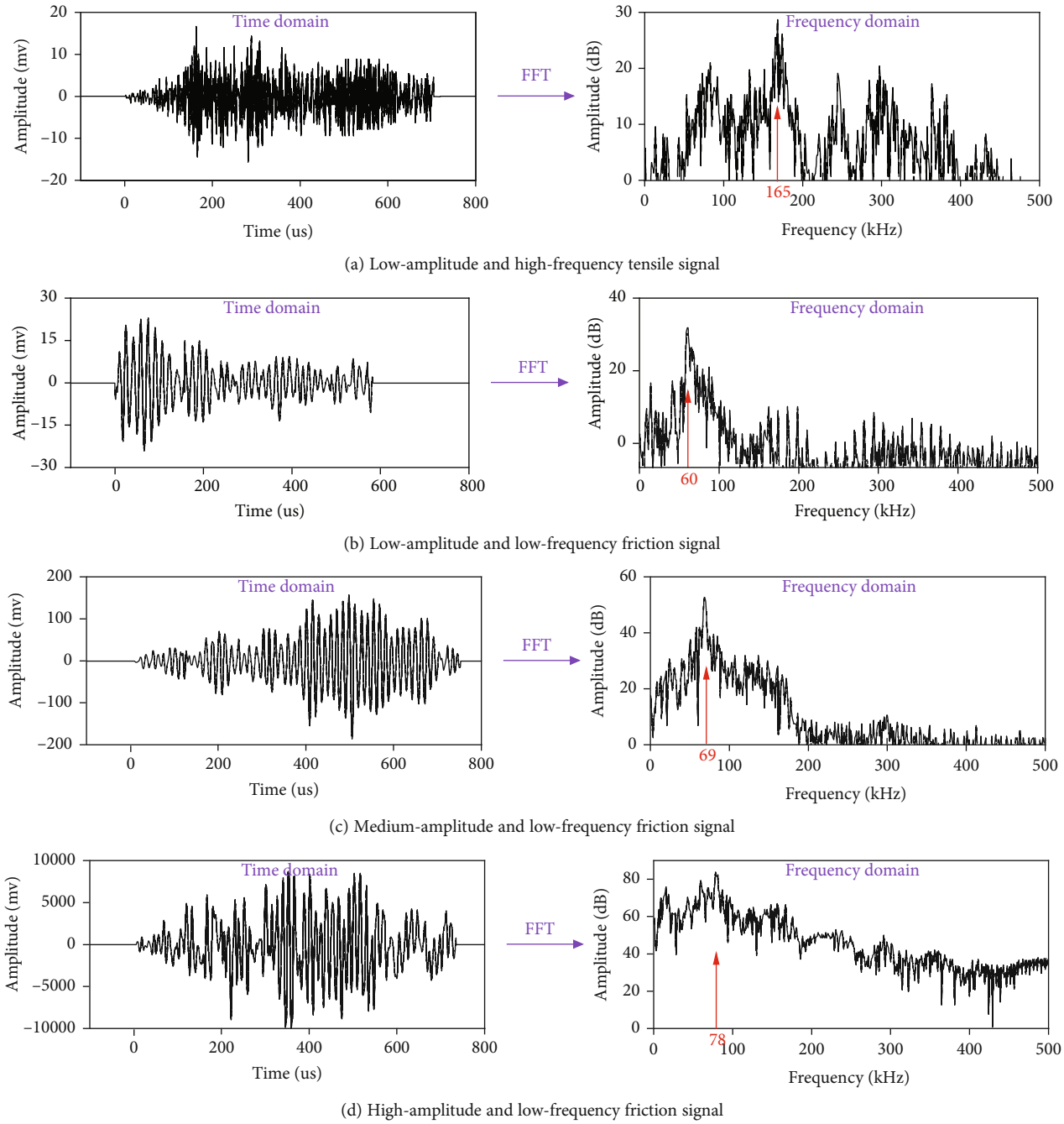

Figure 14: Typical AE waveform and spectrum signals of rock joints under direct shear test.

into three amplitude types: low amplitude, medium amplitude, and high amplitude, as shown in Figures 14(b), 14(c) and 14(d), which represent the friction behaviors between cracks or joint contact surfaces. The low-amplitude, low-frequency signals and medium-amplitude, low-frequency signals are mostly generated during the whole shear test, accompanied by a few slight friction sounds. The high-amplitude, low-frequency signals usually occur at the end moment of the experiment, accompanied by a violent sound, and the signal amplitude is thousands or hundreds of times that of the low-amplitude signal.

4. Discussion

It is generally believed that rock damage is a gradual process, from the early, middle, and final stages of damage, including rock crack initiation, propagation, friction, and fracture deformation mechanisms. These deformation processes of cracks are released with different energy intensities and accompanied by different acoustic emission signal characteristics. In the initiation stage of cracks, sliding friction and intergranular slip are formed between rock particles, resulting in low-amplitude and low-energy friction signals. As

Table 5: Acoustic emission spectrum characteristics in different failure forms of rocks.

Test types	Rock types	Dominant frequency distribution/kHz	Frequency spectrum characteristics	References
Uniaxial compression test	Sandstone	10-70 kHz (much) 120-180 kHz (few)	As the test progresses, low frequency increases, high frequency decreases	Wang et al. [30]
True triaxial compression test	Limestone	60-110 kHz, 170-190 kHz	Low-amplitude and high-frequency signal (low stress) High-amplitude and low-frequency signal (high stress)	He et al. [28]
Direct tensile test	Marble	14-86 kHz, 200-268 kHz (more than 90%)	Tensile failure is more than shear failure	Li et al. [33]
Brazil tensile test	Shale	100–150 kHz (60.02%) 150–250 kHz (11.26%) 250–350 kHz (28.72%)	Friction signal Shearing signal Tensile (tearing) signal	Ban et al. [34]
Three-point bending test	Concrete	50-250 kHz	High frequency (microcracks) Low frequency (macrocracks)	Chen et al. [36]
Joint shear test	Skarn	5~35 kHz (less than 5%) 35~122 kHz (more than 90%) 122~170 kHz (less than 5%)	Low-amplitude and high-frequency signal (low stress) High-amplitude and low-frequency signal (high stress)	This paper

the cracks grow, weak tensile signals and medium friction-type signals are generated. Until the end of loading, macroscopic large-scale cracks are formed, and the friction is intensified, and high-amplitude and high-energy acoustic emission signals are mostly generated [27].

Through literature research, it can be found that there are some similarities and differences between rock shear failure and other forms of rock failure. These failure modes include rock uniaxial compression test, direct tensile test, Brazil tensile test, and three-point bending test, and their acoustic emission peak frequency characteristics of damage are shown in Table 5. The acoustic emission frequency band of rock failure is mainly in the range of 0-400 kHz. When the rock is compressed and sheared, its frequency band is mostly in the range of low frequency, and as the load increases, the high-frequency signal gradually decreases, and the low-frequency signal gradually increases; when the rock is under tension, the proportion of high frequency is obviously more than that of the rock under compression and shear. It is worth noting that no matter the rock is under compression, shear, or tension, macroscopic large cracks are formed when the rock is broken, and high-amplitude, low-frequency acoustic emission signals are formed. This signal feature has a certain guiding significance for the precursor information identification of rock failure.

In this article, the issue of setting the ratio of the acoustic emission parameter RA value to the AF value needs further discussion. In the next study, we can set the ratio value to 1 : 1, 1 : 5, 1 : 20, 1 : 50, or 1 : 100, rely on these ratios to distinguish the tensile signal from the shear signal, and analyze these signal evolution trends.

In summary, as an accompanying phenomenon in the rock failure process, rock acoustic emission contains a lot of information about the internal failure process of rocks. Acoustic emission technology, as a prediction method of rock microcracks and expansion, has an important value in monitoring the occurrence of rock or rock mass destruction and earthquake prediction [47]. After having a preliminary understanding of the shear acoustic emission behaviors of rock joints, we can apply it to the monitoring and forecasting of rock mass stability and safety issues in metal mines, coal mines, tunnel engineering, and slope engineering.

5. Conclusions

By processing and analyzing the AE signal, the shear failure behaviors of rock joints under different normal stress were studied from the point of view of tensile and shear crack signals, and the following four conclusions are obtained.

(1) Under cyclic shearing load, the stress-displacement curve forms several cyclic hysteresis loops, and the number of hysteresis loops increases with the increase of normal stress. The shear strength of each curve is about 70%~80% of the corresponding normal stress

(2) There are obvious Kaiser effect and Felicity effect in the multistage cyclic shear conditions of rock joint. The Felicity ratio is greater than 1 at the early stage and less than 1 at the later stage. The Kaiser effect of rock joints indicates that rock has the ability to remember shear deformation, and the Felicity effect indicates that rock produces an irreversible damage

(3) With the proportional classification method of RA value and AF value, it is easy to distinguish the acoustic emission signals of tensile crack and shear crack in the joint shear process and the evolution characteristics of that two signals. The spectrum distribution diagram of acoustic emission shows that its peak frequency has three frequency bands: high, medium, and low, which are distributed in the range of 0~35 kHz, 35~122 kHz, and 122~300 kHz, respectively. Both low-frequency and high-frequency signals account for less than 10%, and medium-frequency signals account for more than 90%

(4) By performing the fast Fourier transform (FFT) on the AE waveform signals, we can obtain the frequency domain information of the waveform signals.

There are one type of tensile signal and three types of friction signals in the shearing process. The tensile signal has the characteristics of high frequency and low amplitude, and the friction signal has the characteristics of low frequency and low amplitude, low frequency and medium amplitude, and low frequency and high amplitude

Data Availability

The experimental data used to support the findings of this study are included within the article.

Conflicts of Interest

The authors declare no conflict of interest.

Acknowledgments

The authors would like to thank the editors and the anonymous reviewers for their helpful and constructive comments. This work was supported by the National Key Technologies Research and Development Program of China (2018YFC0808402) and Fundamental Research Funds for the Central Universities (FRF-TP-20-004A2 and 06500072).

References

[1] T. Wu, Y. Cai, L. Guo, D. Ling, and J. Wang, "Influence of shear stress level on cyclic deformation behaviour of intact Wenzhou soft clay under traffic loading," *Engineering Geology*, vol. 228, pp. 61–70, 2017.

[2] Z. G. Tao, C. Zhu, X. H. Zheng, and M. C. He, "Slope stability evaluation and monitoring of Tonglushan ancient copper mine relics," *Advances in Mechanical Engineering*, vol. 10, no. 8, 2018.

[3] Z. G. Tao, C. Zhu, M. C. He, and M. Karakus, "A physical modeling-based study on the control mechanisms of Negative Poisson's ratio anchor cable on the stratified toppling deformation of anti- inclined slopes," *International Journal of Rock Mechanics and Mining Sciences*, vol. 138, article 104632, 2021.

[4] E. J. Kaiser, *An Investigation into the Occurrence of Noises in Tensile Tests or a Study of Acoustic Phenomena in Tensile Tests, [Ph.D thesis]*, Dissertation Technische Hochschule Munchen, Munich, 1950.

[5] H. M. Tensi, "The Kaiser–effect and its scientific background," *Journal of Acoustic Emission*, vol. 22, pp. s1–s16, 2004.

[6] R. E. Goodman, "Subaudible noise during compression of rocks," *Geological Society of America Bulletin*, vol. 74, no. 4, pp. 487–490, 1963.

[7] D. J. Holcomb, "General theory of the Kaiser effect," *International Journal of Rock Mechanics and Mining Sciences & Geomechanics Abstracts*, vol. 30, no. 7, pp. 929–935, 1993.

[8] A. Lavrov, "Kaiser effect observation in brittle rock cyclically loaded with different loading rates," *Mechanics of Materials*, vol. 33, no. 11, pp. 669–677, 2001.

[9] A. Lavrov, "The Kaiser effect in rocks: principles and stress estimation techniques," *International Journal of Rock Mechanics and Mining Sciences*, vol. 40, no. 2, pp. 151–171, 2003.

[10] A. Lavrov, "Fracture–induced physical phenomena and memory effects in rocks: a review," *Strain*, vol. 41, no. 4, pp. 135–149, 2005.

[11] M. A. Hamstad, "Discussion of the basic understanding of the Felicity effect in fiber composites," *Journal of Acoustic Emission*, vol. 5, no. 2, pp. 95–102, 1986.

[12] Y. Zhang, Y. Chen, R. Yu, L. Hu, and M. Irfan, "Effect of loading rate on the Felicity effect of three rock types," *Rock Mechanics and Rock Engineering*, vol. 50, no. 6, pp. 1673–1681, 2017.

[13] Y. Chen, M. Irfan, and C. Song, "Verification of the Kaiser effect in rocks under tensile stress: experiment using the Brazilian test," *International Journal of Geomechanics*, vol. 18, no. 7, article 04018001, 2018.

[14] ASTM International, *E1067/E1067M-18 Standard Practice for Acoustic Emission Examination of Fiberglass Reinforced Plastic Resin (FRP) Tanks/Vessels*, ASTM International, West Conshohocken, PA, 2018.

[15] Y. Filimonov, A. Lavrov, Y. Shafarenko, and V. Shkuratnik, "Observation of post–failure Kaiser effect in a plastic rock," *Pure and Applied Geophysics*, vol. 159, no. 6, pp. 1321–1331, 2002.

[16] Q. Meng, Y. Chen, M. Zhang, L. Han, H. Pu, and J. Liu, "On the Kaiser effect of rock under cyclic loading and unloading conditions: insights from acoustic emission monitoring," *Energies*, vol. 12, no. 17, article 3255, 2019.

[17] W. G. Liang, Y. S. Zhao, S. G. Xua, and M. B. Dusseaultb, "Effect of strain rate on the mechanical properties of salt rock," *International Journal of Rock Mechanics and Mining Sciences*, vol. 48, no. 1, pp. 161–167, 2011.

[18] A. Lavrov, A. Vervoort, M. Wevers, and J. A. L. Napier, "Experimental and numerical study of the Kaiser effect in cyclic Brazilian tests with disk rotation," *International Journal of Rock Mechanics and Mining Sciences*, vol. 39, no. 3, pp. 287–302, 2002.

[19] V. Leelalerkiet, T. Shimizu, Y. Tomoda, and M. Ohtsu, "Estimation of corrosion in reinforced concrete by electrochemical techniques and acoustic emission," *Journal of Advanced Concrete Technology*, vol. 3, no. 1, pp. 37–147, 2005.

[20] M. Wang, C. Tan, J. Meng, B. Yang, and Y. Li, "Crack classification and evolution in anisotropic shale during cyclic loading tests by acoustic emission," *Journal of Geophysics and Engineering*, vol. 14, no. 4, pp. 930–938, 2017.

[21] C. V. Steen, L. Pahlavan, M. Wevers, and E. Verstrynge, "Localisation and characterisation of corrosion damage in reinforced concrete by means of acoustic emission and X–ray computed tomography," *Construction and Building Materials*, vol. 197, pp. 21–29, 2019.

[22] Y. Wang, B. Zhang, S. H. Gao, and C. H. Li, "Investigation on the effect of freeze-thaw on fracture mode classification in marble subjected to multi-level cyclic loads," *Theoretical and Applied Fracture Mechanics*, vol. 111, article 102847, 2021.

[23] Z. H. Zhang and J. H. Deng, "A new method for determining the crack classification criterion in acoustic emission parameter analysis," *International Journal of Rock Mechanics and Mining Sciences*, vol. 130, article 104323, 2020.

[24] X. L. Li, "A brief review: acoustic emission method for tool wear monitoring during turning," *International Journal of Machine Tools & Manufacture*, vol. 42, no. 2, pp. 157–165, 2002.

[25] M. E. Malandro, "Fast Fourier transforms for finite inverse semigroups," *Journal of Algebra*, vol. 324, no. 2, pp. 282–312, 2010.

[26] W. B. Yao, C. Y. Dai, W. G. Mao, C. Lu, L. Yang, and Y. C. Zhou, "Acoustic emission analysis on tensile failure of air plasma–sprayed thermal barrier coatings," *Surface & Coatings Technology*, vol. 206, no. 18, pp. 3803–3807, 2012.

[27] M. Ohnaka and K. Mogi, "Frequency characteristics of acoustic emission in rocks under uniaxial compression and its relation to the fracturing process to failure," *Journal of Geophysical Research-Solid Earth*, vol. 87, no. B5, pp. 3873–3884, 1982.

[28] M. C. He, J. L. Miao, and J. L. Feng, "Rock burst process of limestone and its acoustic emission characteristics under true–triaxial unloading conditions," *International Journal of Rock Mechanics and Mining Sciences*, vol. 47, no. 2, pp. 286–298, 2010.

[29] Z. Song, T. Frühwirt, and H. Konietzky, "Characteristics of dissipated energy of concrete subjected to cyclic loading," *Construction and Building Materials*, vol. 168, pp. 47–60, 2018.

[30] C. Y. Wang, X. K. Chang, Y. L. Liu, and S. J. Chen, "Mechanistic characteristics of double dominant frequencies of acoustic emission signals in the entire fracture process of fine sandstone," *Energies*, vol. 12, article 3959, 2019.

[31] W. R. Liu, J. K. Liu, and C. Zhu, "Multi-scale effect of acoustic emission characteristics of 3D rock damage," *Arabian Journal of Geosciences*, vol. 12, no. 22, p. 668, 2019.

[32] Y. Wang, W. K. Feng, H. J. Wang, C. H. Li, and Z. Q. Hou, "Rock bridge fracturing characteristics in granite induced by freeze-thaw and uniaxial deformation revealed by AE monitoring and post-test CT scanning," *Cold Regions Science and Technology*, vol. 177, article 103115, 2020.

[33] L. R. Li, J. H. Deng, L. Zheng, and J. F. Liu, "Dominant frequency characteristics of acoustic emissions in white marble during direct tensile tests," *Rock Mechanics & Rock Engineering*, vol. 50, no. 5, pp. 1337–1346, 2017.

[34] Y. Ban, X. Fu, and Q. Xie, "Revealing the laminar shale microdamage mechanism considering the relationship between fracture geometrical morphology and acoustic emission power spectrum characteristics," *Bulletin of Engineering Geology and the Environment*, vol. 79, no. 2, pp. 1083–1096, 2020.

[35] N. Gong, S. W. Hu, X. D. Chen, X. Q. Fan, and X. N. Cai, "Fracture behavior and acoustic emission characteristics of reinforced concrete under mixed mode I-II load conditions," *Theoretical and Applied Fracture Mechanics*, vol. 109, article 102770, 2020.

[36] X. Chen, D. Shi, J. Zhang, and X. Cheng, "Experimental study on loading rate and notch-to-depth ratio effects on flexural performance of self-compacting concrete with acoustic emission and digital image correlation technologies," *The Journal of Strain Analysis for Engineering Design*, vol. 56, no. 3, pp. 148–160, 2021.

[37] Q. S. Liu, Y. C. Tian, D. F. Liu, and Y. L. Jiang, "Updates to JRC-JCS model for estimating the peak shear strength of rock joints based on quantified surface description," *Engineering Geology*, vol. 228, no. 10, pp. 282–300, 2017.

[38] J. Muralha, G. Grasselli, B. Tatone, M. Blümel, P. Chryssanthakis, and Y. Jiang, "ISRM suggested method for laboratory determination of the shear strength of rock joints: revised version," *Rock Mechanics and Rock Engineering*, vol. 47, no. 1, pp. 291–302, 2014.

[39] D. A. Lockner, "The role of acoustic emission in the study of rock fracture," *International Journal of Rock Mechanics and Mining Sciences & Geomechanics Abstracts*, vol. 30, no. 7, pp. 883–899, 1993.

[40] M. Ohtsu, "The history and development of acoustic emission in concrete engineering," *Magazine of Concrete Research*, vol. 48, no. 4, pp. 321–330, 1996.

[41] G. Manthei, J. Eisenblätter, and T. Spies, "Acoustic emission in rock mechanics studies," in *Acoustic Emission–Beyond the Millennium*, T. Kishi, M. Ohtsu, and S. Yuyama, Eds., pp. 127–144, Elsevier, 2000.

[42] Non–destructive testing (ISO 12716:2001), *Acoustic Emission Inspection*, Vocabulary, 2001.

[43] M. Ohtsu, T. Isoda, and Y. Tomoda, "Acoustic emission techniques standardized for concrete structures," *Journal of Acoustic Emission*, vol. 25, pp. 21–32, 2007.

[44] M. Ohtsu, *Acoustic Emission Testing*, Springer, Berlin Heidelberg, 2008.

[45] K. Ohno and M. Ohtsu, "Crack classification in concrete based on acoustic emission," *Construction & Building Materials*, vol. 24, no. 12, pp. 2339–2346, 2010.

[46] G. Wang, Y. Zhang, Y. Jiang et al., "Shear behaviour and acoustic emission characteristics of bolted rock joints with different roughnesses," *Rock Mechanics and Rock Engineering*, vol. 51, no. 6, pp. 1885–1906, 2018.

[47] R. Jiang, F. Dai, Y. Liu, and A. Li, "Fast marching method for microseismic source location in cavern-containing rockmass: performance analysis and engineering application," *Engineering*, 2021.